Int. J. Electrochem. Sci., 15 **(2020)** 10994 – 11007, doi: 10.20964/2020.11.43

International Journal of
ELECTROCHEMICAL
SCIENCE
www.electrochemsci.org

Corrosion Behavior of X100 Pipeline Steel and Its Heat-Affected Zones in Simulated acidic Soil Solution

Yong Yang, Xiushan Shi, Ming Sun, Weiguo Zeng[*]

China Special Equipment Inspection and Research Institute, Beijing 100029, China
[*]E-mail: 39530354@qq.com

Received: 18 June 2020 / *Accepted:* 13 August 2020 / *Published:* 30 September 2020

Different thermal cycle times, peak temperatures, and cooling rates were used in a Gleeble thermomechanical processing machine to simulate the coarse-grained heat-affected zones (CGHAZ) and inter-critically reheated coarse-grained heat-affected zones (ICCGHAZ) of X100 pipeline steel. The corrosion behavior of the X100 pipeline base steel and the heat-affected zones (HAZs) were studied in a simulated acidic soil solution. Open circuit potential (OCP) measurements, potentiodynamic polarization, electrochemical impedance spectroscopy (EIS), scanning electron microscopy (SEM), energy dispersive x-ray spectroscopy (EDS), and weight loss testing were used to characterize the corrosion behavior of X100 pipeline steel and its CGHAZ and ICCGHAZ in a simulated acidic soil solution. The microstructures of the CGHAZ and ICCGHAZ were found to be significantly different from that of the base steel. The original X100 pipeline steel showed the most positive OCP, the lowest polarization resistance, and the highest corrosion rate. The ICCGHAZ showed the most negative OCP, but CGHAZ showed the highest polarization resistance and the lowest corrosion rate. The corrosion products of X100 pipeline steel base material, CGHAZ and ICCGHAZ all form a layer covered with cracks, which provides poor protection for the substrate. Immersed in a simulated acidic soil solution, the X100 pipeline steel base metal samples were uniformly corroded, while CGHAZ and ICCGHAZ suffered severe intergranular corrosion.

Keywords: X100 pipeline steel, Heat-Affected Zones, corrosion behavior, simulated acidic soil solution, intergranular corrosion

1. INTRODUCTION

The transformation of oil and gas pipelines to large- diameter, high-pressure, and large-volume systems puts forward higher requirements on the strength and toughness of pipeline steel [1]. The higher performance of high-strength X100 pipeline steel gives it great application prospects [2]. At present, X100 pipeline steel trials have been carried out to verify the relevant technical specifications [3]. Studies have shown that high-strength pipeline steels such as X100 have a greater risk of failure than low-strength pipeline steels when they are subjected to long-term corrosion [4]. The process of on-site construction makes the external anti-corrosion coating at the welding joint become the weak point of the corrosion protection system for the entire pipeline. The difference in microstructure among the HAZ, the base metal, and the fusion zone of the weld seam makes the welded joint more likely to produce local corrosion, cracks, and other defects that endanger pipeline safety [5, 6]. Previous studies [7-11] showed that the microstructure of the HAZ has a very large influence on the corrosion behavior of high-strength pipeline steel, although the result of this influence depends on the types of steel and the corrosive environments. In different corrosive media, the HAZs sometimes have better corrosion resistance than the base metal, but sometimes it is the opposite. Southeast China is a densely populated and economically developed region, with a large number of oil and gas pipelines. The Yingtan red soil in the southeastern region is a typical acidic soil with high temperature, air proof, high water content, and low oxygen content, with a pH value of 3-5, which is extremely corrosive to the buried pipelines [12].

The microstructure and performance of the CGHAZ and ICCGHAZ of X100 pipeline steel welded joints have been widely studied [13-16]. However, the corrosion characteristics of these HAZs of X100 pipeline steel in acid soil environments are rarely studied. In this paper, thermal processing of the X100 pipeline steel samples was performed to obtain the CGHAZ and ICCGHAZ microstructure using the Gleeble 3500 thermomechanical processing machine with different thermal peak temperatures, cooling rates and cycle times. Open circuit potential (OCP) measurements, potentiodynamic polarization, electrochemical impedance spectroscopy (EIS), scanning electron microscopy (SEM), energy dispersive x-ray spectroscopy (EDS) and weight loss testing were employed to characterize the corrosion behavior of the X100 pipeline steel and its CGHAZ and ICCGHAZ in a simulated Yingtan acidic soil solution. The research results provide a theoretical basis for the corrosion protection of X100 pipeline steel in the future.

2. EXPERIMENTAL

2.1 Materials and solutions

All samples investigated in this work were machined from an API X100 pipeline steel plate with a chemical composition (wt %): C 0.051, Mn 1.909, Si 0.216, P 0.010, S 0.004, Ni 0.313, Cr 0.287, Cu 0.139, Al 0.045, Mo 0.250, Nb 0.063, Ti 0.012, V 0.039, Pb 0.002, B 0.0003, Sn 0.003, As 0.005, and Fe balance. Thermal simulation processing of the samples was performed to obtain CGHAZ and ICCGHAZ microstructures using the Gleeble 3500 thermomechanical processing machine (DSI, USA) under the repetitive thermal cycles presented in Fig. 1 [15-16]. After the thermal simulation was complete, the samples of X100 pipeline steel as-received, CGHAZ and ICCGHAZ were ground and polished, then eroded with 4% nitric acid alcohol solution, and the microstructure observed under an optical microscope (Zeiss Stereo Microscopy). The microstructure of CGHAZ and ICCGHAZ is significantly different from that of the original X100 Pipeline Steel, and is described in detail in reference 16.

The test solution used for this study was a simulated acidic soil solution containing [17]: 0.222g/L

$CaCl_2$, 0.936g/L NaCl, 0.284g/L Na_2SO_4, 0.394 g/L $MgSO_4{\cdot}7H_2O$, 0.586g/L KNO3, 0.302g/L $NaHCO_3$ made from analytic grade reagents and deionized water. The pH of the solution was adjusted to 4.1 by adding NaOH and acetic acid solutions.

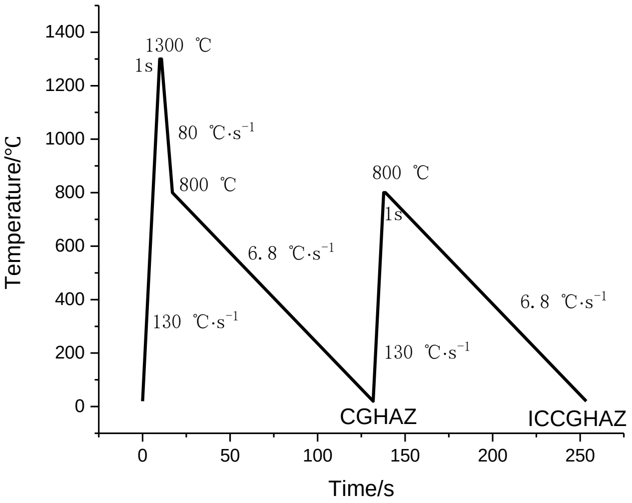

Figure 1. Thermal cycle temperature recordings by Gleeble 3500

2.2 The immersion test and electrochemical measurements

The cutting surface, dimensions, and working area of the HAZ samples used in the corrosion experiment are shown in Fig. 2. The handling process of the samples was the same as described in Reference 16. The samples used for weight loss testing were immersed in simulated acidic soil solution for 450 hours. Before and after the immersion, the samples for weight loss test were weighed with a high-precision electronic balance, and then the average corrosion rate was calculated. All immersion and electrochemical experiments were conducted in a sealed cell. Before the start of the immersion test, high-purity N_2 (99.999%) was blown into the soil simulation solution for about one hour to remove dissolved oxygen, and the solution was kept isolated from air during the test process. The temperature of immersion test was room temperature (about 20 - 30℃).The samples, experimental process, and data processing of the electrochemical experiment were the same as those described in Reference 16. Before the electrochemical experiment, the soil simulation solution was purged with N_2 to remove dissolved oxygen for about 3 hours, then N_2 was passed into the space above the liquid surface in closed cell to maintain the solution in a deoxygenated state. The temperature of the electrochemical experiment was controlled at 25±1℃ by a constant temperature water bath.

3. RESULTS AND DISCUSSION

3.1 Electrochemical characterization

3.1.1 OCP

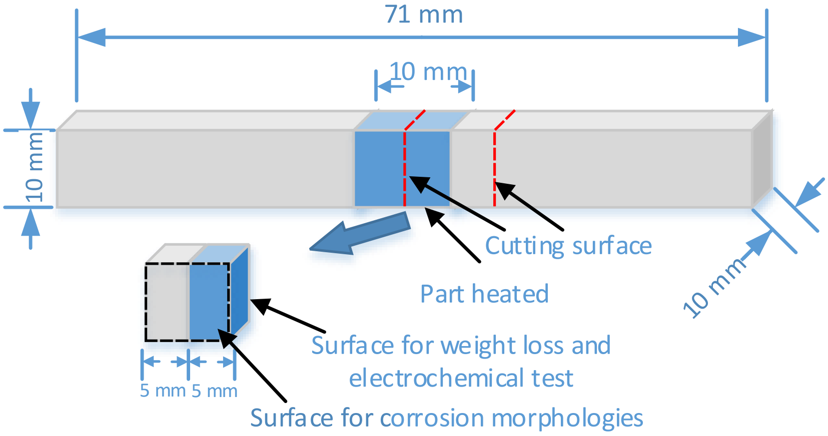

Figure 2. Schematic diagram of the research sample

The time dependence of OCP for X100 base steel, CGHAZ, and ICCGHAZ is shown in Fig. 3. All samples showed similar OCP–time profiles. The OCP stabilized quickly after a rapid decline within the first 0.5 h. When the immersion time was longer than 1.5 hours, the OCP of the base steel remained the most positive, and the OCP of the ICCGHAZ was the most negative, which was the same as the OCP distribution of the X60~X80 pipeline steel base material and HAZ in a previous study [7-11]. Bainite is a mixture of ferrite and small island-like structures surrounded by ferrite [18]. The area of the ferrite structures in the HAZ samples was larger than that of the ferrite structure in the base material [16]. Since the natural corrosion potential of ferrite is generally lower than the potential of other microstructures [19, 20], the anodic current density generated by ferrite is greater than the average anodic current density of other microstructures when the mixed potential is unchanged. Then, when the reaction area of the ferrite increases, the anodic current will become larger, while the total current of the cathode reaction will not change. Therefore, in order to maintain current balance, the OCP is driven negative, increasing the overpotential of the cathode reaction and reducing the overpotential of the anode reaction, thereby increasing the cathode reaction current and reducing the anode reaction current to achieve a new current balance. After purging N_2 into the space above the liquid surface instead of the solution, all three OCPs moved negatively quickly, which might be related to the effect of solution vibration on the deposition of corrosion products caused by N_2 and the influence of the diffusion of N_2 in the solution on the surface environment of the samples.

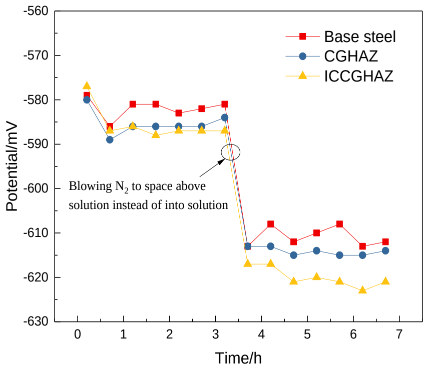

Figure 3. OCP vs immersion time of samples in a simulated acidic soil solution

3.1.2 Potentiodynamic polarization

Fig. 4 shows the potentiodynamic polarization curves of base steel, CGHAZ, and ICCGHAZ samples under the conditions of the present study. The polarization curves of the base steel, CGHAZ, and ICCGHAZ immersed for different durations in the soil simulation solution showed roughly similar characteristics: typical active dissolution and no passivation in the anode potential region. The cathodic polarization curves for 8 and 30 hours of immersion showed diffusion control characteristics, and the corrosion current density of the polarization curve was significantly greater than that of the sample subjected to 485 hours of immersion. Since O_2 had been removed from the soil simulation solution, the cathodic reaction included mainly the processes given in formulas (1)-(3) [21]. The diffusion control characteristics when the current density is large in the early stages of immersion are caused by the diffusion of reactive ions. In the later stages of immersion, the reaction changes to activation control, as shown by a decrease in current density. Table 1 shows the corrosion current densities fitted from the polarization curves. When immersed for 8 hours, the CGHAZ showed the largest corrosion current density, followed by the base material, and finally ICCGHAZ. When immersed for 30 hours, the corrosion current density of CGHAZ does not change much, while those of the other samples increased greatly, and the corrosion current densities of all three types of samples were not significantly different. When immersed for 485 hours, the corrosion current densities of the samples decreased to less than those of the samples immersed for 8 hours, and the corrosion current density of base material became the largest while that of the CGHAZ became the smallest. The corrosion current density increased in the early stages of immersion and decreased in the later stages. Previous studies [22, 23] believed that the thin and uneven granular corrosion products formed on the surface of the sample in the early stages of corrosion increased the cathodic reaction area and promoted corrosion, and corrosion products in the later stage of immersion essentially cover the entire metal surface, which could inhibit corrosion to a certain extent.

$$2H^{+}+2e^{-}\rightarrow H_{2} \tag{1}$$

$$2H_{2}CO_{3}+2e^{-}\rightarrow H_{2}+2HCO_{3}^{-} \tag{2}$$

$$2HCO_{3}^{-}+2e^{-}\rightarrow H_{2}+2CO_{3}^{2-} \tag{3}$$

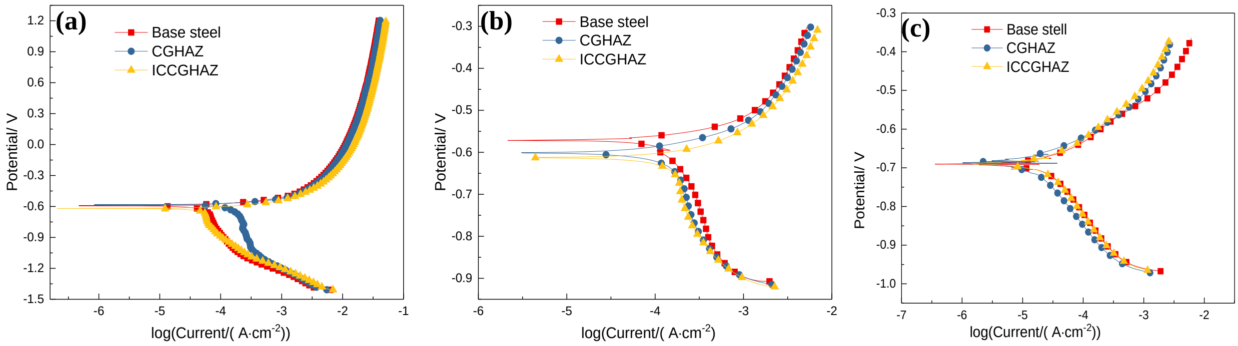

Figure 4. Polarization curves of X100 steel in soil simulating solution with (a) 8h, (b)30h, and (c)485h

Table 1. Corrosion current density fitted by polarization curve

Time	Corrosion current densities(ηA·cm^{-2})		
h	Base steel	CGHAZ	ICCGHAZ
8	14.33	21.53	13.54
30	22.78	22.82	22.25
485	10.53	8.38	9.44

3.1.3 EIS

Figs. 5 shows the Nyquist and Bode plots for X100 base steel, CGHAZ, and ICCGHAZ samples immersed in simulated acidic solution for different times. As can be seen from the figures, the corrosion mechanism and interface interaction properties of base materials, CGHAZ and ICCGHAZ did not vary significantly with immersion time. [24]. The Nyquist diagrams show a capacitive reactance arc shrinking along the real-axis in the low frequency range, indicating the formation of a corrosion product film on the surfaces of the samples that influenced the electrode reaction rate [25]. At the low frequency end, the Nyquist plots of the samples immersed for 8 hours showed an irregular disturbance, which is probably due to the unstable surface morphology of the sample and the instability of the corrosion product film. The disturbance of EIS curves of the sample immersed for 30 hours was alleviated at the low frequency end. The EIS curves of the sample immersed for 485 hours became very regular, indicating that the surfaces of the samples were in a stable state.

It can be deduced from the Nyquist and Bode plots that the time constant of the interface of samples did not exceed two [26]. Based on previous works [24, 26, 27] and the error results fitted by Zsimwin software, the equivalent circuit R(QR) was used to fit the EIS data of the base steel immersed for 8 hours. The equivalent circuit depicted in Fig. 7 was used to fit the rest EIS data; the constant phase element Q_f in the equivalent circuit of CGHAZ and ICCGHAZ immersed for 30 hours is replaced with an equivalent capacitance C_f. The fitting results are listed in Table 2. As shown in Fig. 6 and Table 2, Rs represents the solution resistance, R_f is the corrosion product film resistance, R_{ct} corresponds to the charge transfer resistance of the corrosion process, while constant phase elements (CPE) Q_f and Q_{dl} represent the non-ideal corrosion product film capacitance and the double layer capacitance at the metal/electrolyte interface, respectively. n_f and n_{dl} are the CPE exponents. With increased duration of the immersion time, the charge transfer resistance and corrosion product resistance of the sample first decreased and then increased, and the corresponding corrosion rate firstly increased and then decreased. When immersed for 8 hours, the R_{ct} of the base material is the largest and the Rct of the CGHAZ is the smallest. When immersed for 485 hours, the resistance ($R_{ct}+R_f$) of the base steel becomes the smallest, and that of CGHAZ the largest. The EIS experimental conclusions are consistent with the polarization curve test conclusions. From a thermodynamic viewpoint, the more negative the corrosion potential of the metal in the same solution, the more likely the metal is to corrode. When immersed for 7 hours, the potential of the base metal was more positive than that of CGHAZ and ICCGHAZ, indicating that the base metal had the highest thermodynamic stability at this moment, a result which is consistent with the analysis results of EIS for the base metal and HAZs soaked for 8 hours. However, the thermodynamic stability of CGHAZ and ICCGHAZ immersed for 7 hours did not corroborate the EIS result of the samples immersed for 8 hours, which may be related to the fact that the immersion time was not exactly the same and the surface of the sample was not stable. After a long immersion time, although the resistance of the corrosion product of the sample increased, it was still relatively small, so the corrosion products in the Yingtan acidic soil simulating solution had minimal effect on the protection of the substrate.

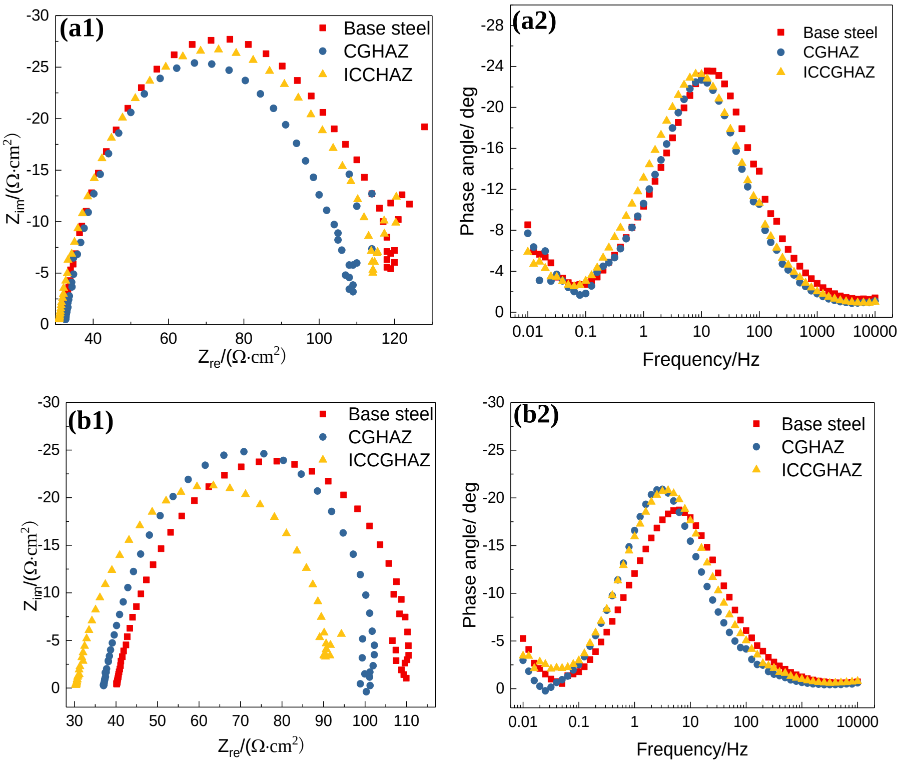

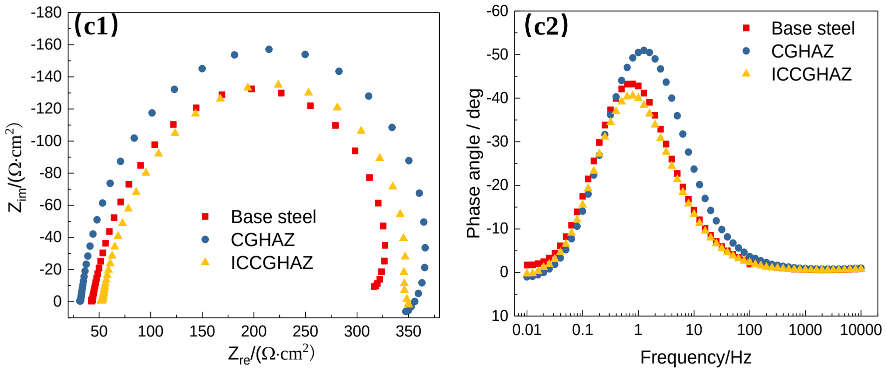

Figure 5. Plots of EIS for X100 in soil simulating solution for (a1, a2) 8h, (b1, b2)30h, and (c1, c2)485h

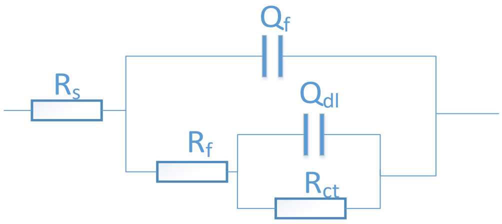

Figure 6. Equivalent circuit of EIS for X100 test samples in soil simulating solution

Table 2. Equivalent circuit fitting for the EIS data of samples

Time (h)	Microstructures	R_s (Ω•cm^2)	Y_f / C_f (Ss^n/cm^2)/ (F/cm^2)	n_f	R_{fs} (Ω•cm^2)	Y_{dl} (Ss^n/cm^2)	n_{dl}	R_{ct} (Ω•cm^2)	Chi-square
8	Base steel	31	—	—	—	9.778×10^{-4}	0.71	90.3	7.288×10^{-4}
	CGHAZ	32	—	—	—	1.200×10^{-3}	0.74	78.1	6.585×10^{-4}
	ICCGHAZ	30	—	—	—	5.676×10^{-3}	0.71	87.7	8.969×10^{-5}
30	Base steel	40	1.174×10-3	0.80	15	4.147×10^{-3}	1.0	56	2.467×10^{-4}
	CGHAZ	37	5.848×10-4	—	11	2.074×10^{-3}	0.81	54	2.087×10^{-4}
	ICCGHAZ	29	3.131×10-4	—	10	2.541×10^{-3}	0.76	63	2.114×10^{-4}
485	Base steel	43	1.403×10^{-3}	0.95	70	1.064×10^{-3}	0.97	218	4.164×10^{-4}
	CGHAZ	32	1.028×10^{-3}	0.97	102	6.379×10^{-4}	099	231	8.58×10^{-4}
	ICCGHAZ	53	1.27×10^{-3}	0.95	89	1.05×10^{-3}	0.98	210	4.953×10^{-4}

3.2 Corrosion rate

The average corrosion rate of the X100 pipeline steel base material, CGHAZ, and ICCHAZ samples after immersion for 450 hours obtained through weight loss experiments is shown in Fig. 7. The corrosion rate of the base metal is the largest, followed by ICCGAHZ and CGHAZ. Related studies [28, 29] have shown that the rate of corrosion of metals in solution is related to grain size, microstructure uniformity, and solution characteristics. The grains of the base material are more uniform and finer, resulting in a large number of grain boundaries. Most of the atoms at the grain boundary are irregularly arranged, and their energy is generally higher than that in the grain bulk, which makes the atomic activity of the grain boundary higher, and hence the number of active atoms participating in the corrosion reaction increases. Ralston [30] found that the relationship between metal corrosion and grain size can be presented as formula (4):

$$i_{corr} = A + Bd^{-0.5} \tag{4}$$

where the constant A is likely to be a function of the corrosion environment (since the same metal may have a different corrosion rate in different electrolytes for a given grain size), the constant B represents a material property, which will differ according to composition or impurity level, and d is the grain size of the metal.

In a non-passivating environment, B takes a positive value, otherwise it takes a negative value. In the case of passivation, the smaller the grain size the smaller the corrosion current, and the larger the grain the larger the corrosion current, i.e. grain refinement can increase the corrosion resistance. In the case of non-passivation, metal grain refinement will decrease corrosion resistance. Gollapudi [31], through correlation analysis of grain size distribution and corrosion current, reported that the grain size distribution of metal materials has an important effect on metal corrosion. In a passivating environment, metals with a large grain size distribution range are more likely to be corroded. In an active corrosion environment, a larger grain size distribution range can improve metal corrosion resistance. Previous research [7-11, 32, 33] showed that the corrosion resistance of the HAZ of pipeline steel in a slightly acidic solution is better than that of the base material, and the corrosion resistance of the HAZ of pipeline steel in neutral and alkaline solutions is worse than that of the base steel, because the grain size of HAZ is generally larger than that of base steel. This proves that the effect of pipeline microstructure on corrosion is consistent with the research results of Ralston [30] and Gollapudi [31]. The acidic soil simulating solution is highly corrosive, and H^+ in the soil simulating solution facilitating the continuous production of H_2 in the reaction process will destroy the corrosion products and make them non-protective. The reaction activity of atoms at the grain boundary which have higher energy than the atoms in the grain is higher, so the base steel that has more grain boundaries is more susceptible to corrosion than the HAZ [34].

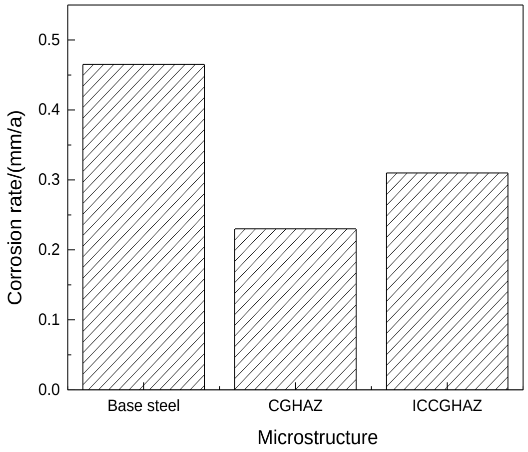

Figure 7. Corrosion rates of base steel, CGHAZ, ICCGHAZ immersed for 450 hours

3.3 Corrosion products

Fig. 8 reveals the morphology of corrosion products of X100 pipeline base material immersed for 90 hours. Fig. 9 shows the X-ray energy spectrum analysis of the lower surface layer of the corrosion product of the X100 pipeline base material immersed for 90 hours. Fig. 10 illustrates the morphology of corrosion products of the base metal, CGHAZ, and ICCGHAZ immersed for about 450 hours. It can be seen that the corrosion products of base steel, CGHAZ and ICCGHAZ formed a relatively thin layer and were covered with cracks, indicating that the corrosion products provided poor protection for the metal substrate, which was consistent with the results of the EIS test. The cracks of the corrosion products of the base metal were mainly parallel, while the cracks of the corrosion products of CGHAZ and ICCGHAZ were mainly ring-shaped, which should be related to microstructural differences. As shown in Fig. 11, the corrosion products are mainly composed of Fe and O. Based on the composition of the soil simulating solution and the corrosion products, it is inferred that the formation process of the corrosion products of X100 pipeline steel in the Yingtan acidic soil simulating solution is as follows [35]:

$$Fe - 2e^{-} \rightarrow Fe^{2+} \tag{5}$$

$$Fe^{2+} + 2HO^{-} \rightarrow Fe(OH)_2 \tag{6}$$

$$Fe(OH)_2 \rightarrow FeOOH + H^{+} + e^{-} \tag{7}$$

Dehydration or reduction of FeOOH will produce corrosion products such as Fe_3O_4 and Fe_2O_3. Due to the generation of hydrogen, a large number of cracks are produced in the corrosion products.

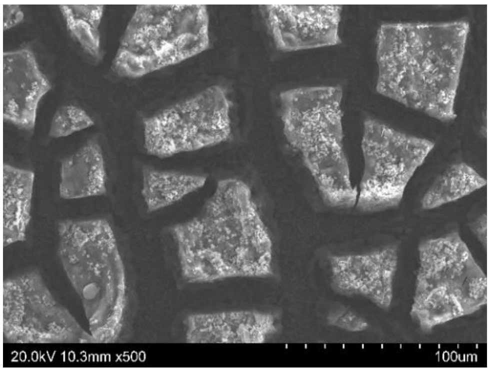

Figure 8 Morphology of corrosion product of base steel for 90h

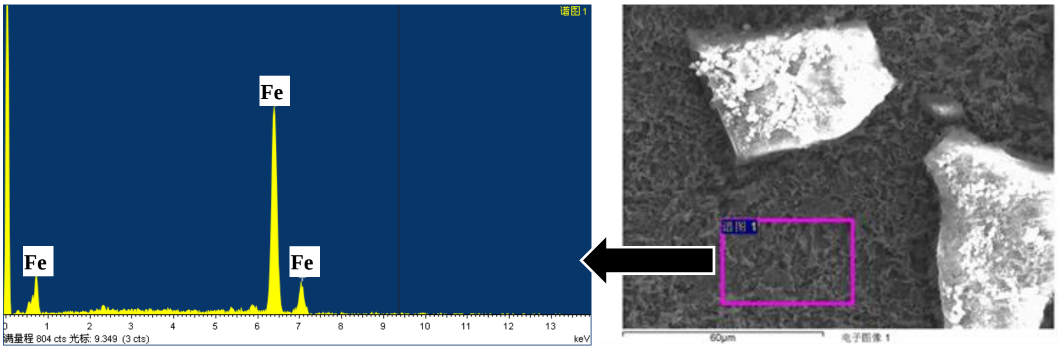

Figure 9 EDS of surface layer under corrosion product

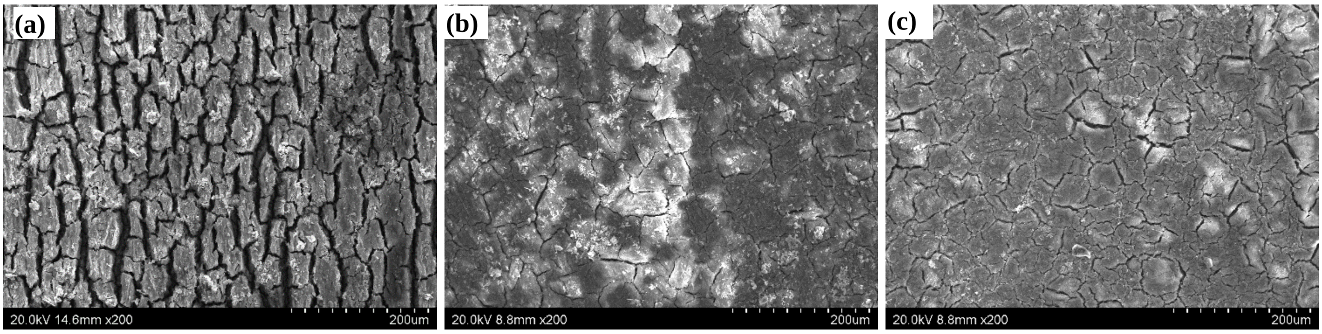

Figure 10. Morphologies of corrosion product of (a) base steel, (b) CGHAZ, and (c) ICCGHAZ immersed for 450h

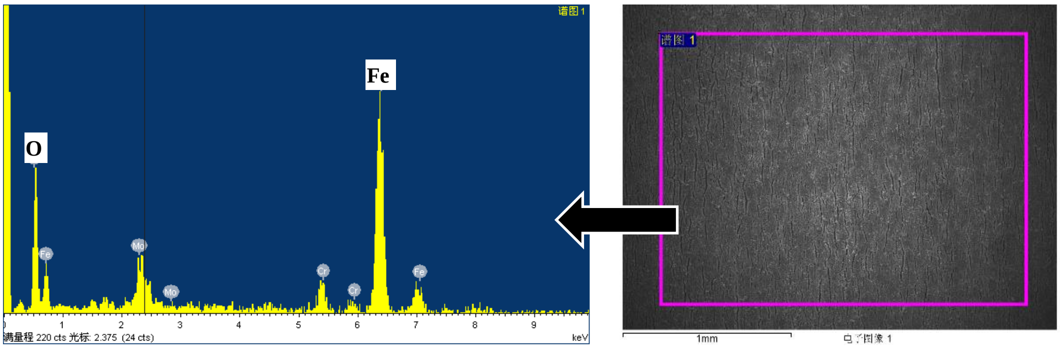

Figure 11. EDS of corrosion product of X100 pipeline steel immersed for 450h

3.4 Corrosion morphologies

The steel surface corrosion morphologies following immersion in the test solution for 40 h are shown in Fig. 12. Fig. 12 a) and b) are taken from the same immersion sample. Fig. 12 c) and d) are taken from the same immersion sample. The corrosion morphology of the base metal is clearly different from that of CGHAZ and ICCGHAZ. A large number of small corrosion pits and holes were distributed across the surface of the base steel, and uniform corrosion is the main feature. The CGHAZ had deep corrosion cracks along the grain boundary, and the corrosion in the grain boundary was groove-shaped. The surface of ICCGHAZ showed ulcer-like corrosion as a whole, and there were obviously more severe corrosion grooves and holes in the original grain boundary of M/A distribution. Fig. 13 shows the corrosion morphology of X100 pipeline steel base material, CGHAZ, and ICCGHAZ immersed in simulated acidic soil solution for 450 hours. It can be seen that all samples were uniformly corroded as a whole; the surface of the base steel was smoother, but there were some smaller corrosion holes. The surface of GCHAZ corroded with a burr-like morphology, and the corrosion degree of the original grain boundary is relatively serious. The surface of ICCGHAZ is still uneven, and the corrosion grooves along the grain boundaries are replaced by a large number of corrosion holes. The reason for the inter-granular corrosion of CGHAZ and ICCGHAZ is that they have higher dislocation density and stronger corrosion reaction activity, because the various trace alloy elements gather at the grain boundary and push the potential at the grain boundary more negative than that in the grain bulk [32 ,34].

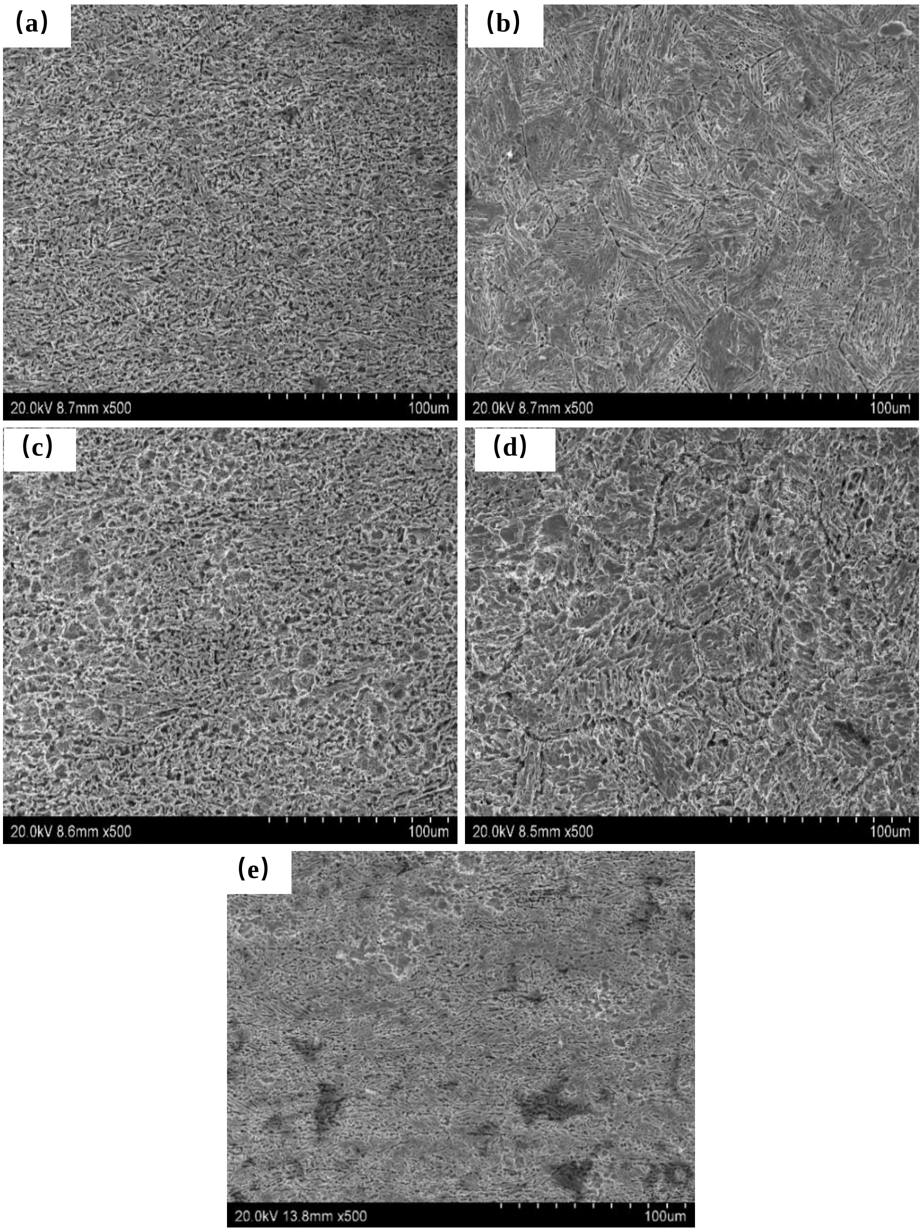

Figure 12. SEM Surface micrographs of (a) base steel adjacent to CGHAZ, (b) CGHAZ, (c) base steel adjacent to ICCGHAZ, (d) ICCGHAZ, and (e) base steel for 40h

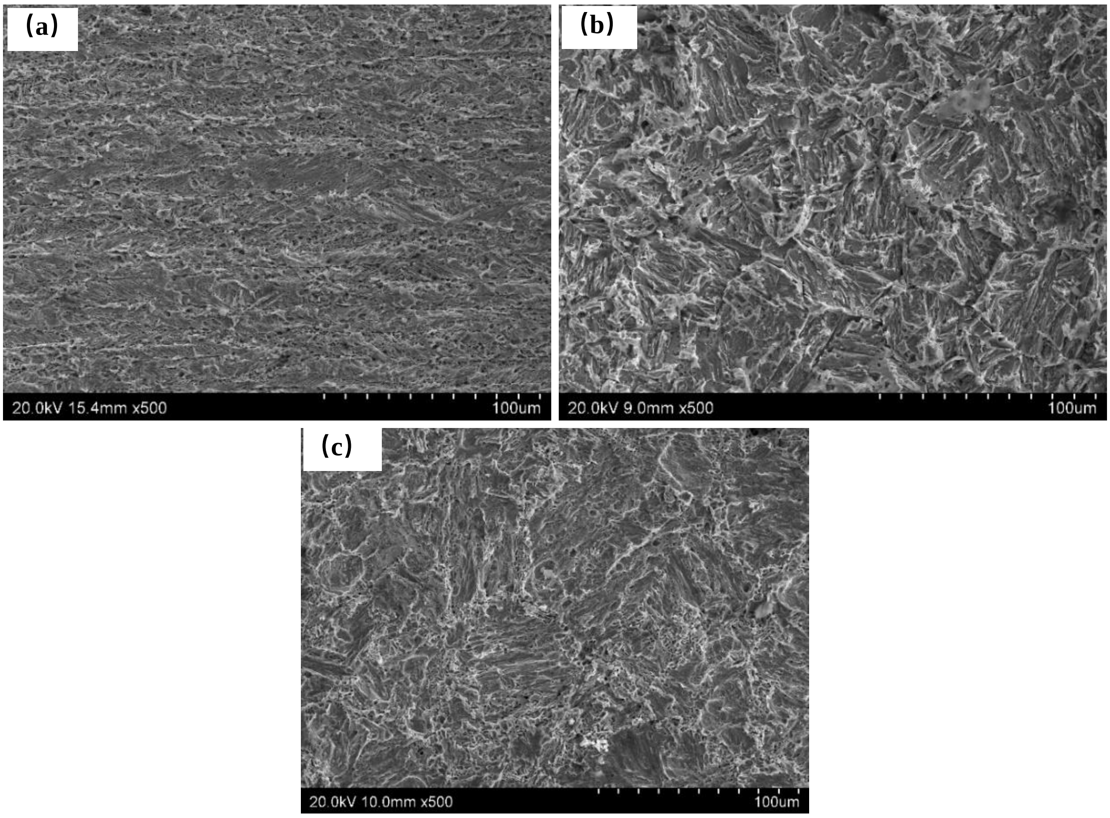

Figure 13. SEM Surface micrographs of (a) base steel, (b) CGHAZ, and (c) ICCGHAZ immersed for 450h

4. CONCLUSIONS

(1) The base material, CGHAZ, and ICCGHAZ of the X100 pipeline steel showed typical active dissolution characteristics in a simulated Yingtan acidic soil solution. The thermodynamic stability of base steel was highest, followed by CGHAZ and ICCGHAZ. The polarization resistance of CGHAZ was largest, followed by base steel and ICCGHAZ. The corrosion rate of the base metal is the largest, which is about 2 times that of CGHAZ and 1.5 times that of ICCGHAZ.

(2) The corrosion products of X100 pipeline steel base material, CGHAZ and ICCGHAZ all form a layer covered with cracks, which provides poor protection for the substrate.

(3) Immersed in Yingtan acidic soil simulating solution, the base steel samples evenly corroded, and CGHAZ and ICCGHAZ suffered severe intergranular corrosion.

ACKNOWLEDGEMENTS
This research was supported by the Science and Technology Plan Projects of State Administration for Market Regulation (2019MK136), CSEI Research Program (2019-Youth-03).

References

1. B. Zhang, C.W. Qian, Y.M. Wang, Y.Z. Zhang, *Pet. Eng. Constr.*, 38 (2012) 1.

2. M. Witek, J. Nat. Gas Sci. Eng., 27 (2015) 374.
3. J. Johnson, M. Hudson, N. Takahashi, M. Nagase, A. Yamamoto, ASME. International Pipeline Conference, 2008 7th International Pipeline Conference, Calgary, Alberta, Canada, 2008, 453.
4. M.A. Maes, M. Dann, M.M. Salama, *Reliab. Eng. Syst. Saf.,* 93 (2008) 447.
5. G. Papadakis, *J. Loss Prevent. Process. Ind.,* 12 (1999) 91.
6. A. Mustapha, E.A. Charles, D. Hardie, *Corros. Sci*., 54 (2012) 5.
7. C.H. Liu, W. Liu, M.X. Lu, *Corros. Sci. Prot. Technol*., 20 (2008) 206.
8. Z. Fan, J.Y. Liu, S.L. Li, T.J. Zhang, *J. Southwest Pet. Univ.(Sci. Tech. Ed.),* 31 (2009) 171.
9. F. Mohammadi, F. F. Eliyan, A. Alfantazi, *Corros. Sci*., 63 (2012) 323.
10. W. Zhao, Y. Zou，Z.D, Zou，K. Matsuda, *Int. J. Electrochem. Sci*., 10 (2015) 9725.
11. C.W. Shi, Y.B. Zhang, P. Liu, Y.L. Xie, *Int. J. Electrochem. Sci.,* 13 (2018) 2412.
12. Z.Y. Liu, G.L. Zhai, C.W. Du, X.G. LI, *Acta Metal. Sin*., 44 (2008) 209.
13. L. Dong, X.Y. Zhang, X.L. Xu, H.L. Gao, *Hot Work. Tech*., 41 (2012) 150.
14. P. Mohseni, J.K. Solberg, M. Karlsen, O.M. Akselsen, E. Stby, *Metall. Mater. Trans*., 45 (2014) 384.
15. X.D. Li, X. Li, S.X. Wang, S.B. Hu, Q.K. He, J.X. Liu, X.Q. Lin, N. Chao, *Heat Treat. Met*., 42 (2017) 66.
16. X.H. Wang, Y. Yang, Y.C. Chen, K.L. Wei, *Int. J. Electrochem. Sci*., 14 (2019) 9181.
17. M. Zhu, J. Ma, Y.F. Yuan, S.M. Yi, G.H. Yu, S.Y. Guo, L. Nie, *T. Mater. Heat Treat*., 39 (2018) 67.
18. X.L. Zhou, H.R. Li, X.Z. Hua, Z.G. Yie, *T. China Welding Inst*., 32 (2011) 37.
19. Y.L. Chao, Y.L. Zhou, S.H. Cheng, Q.S. Sun, Y.B. Liu, *J. Iron Steel Res*., 30 (2018) 489.
20. F.F. Eliyan, A. Akram, *Corros. Sci*., 85 (2014) 380.
21. Z.Y. Liu, C.P. Wang, C.W. Du, X.G. Li, *Acta Metal. Sin*., 47 (2011) 1434.
22. X.Y. Zhang, Z.Q. Shi, Y.F. Wang, M.X. Liu, S.S. Yang, *J. Chin. Soc. Corros. Prot*., 35 (2015) 33.
23. C.M. Xu, Y.Chen, Y.Z. Wang, L.P. Wang, J.H. Lou, *Hot Work. Tech*., 38 (2009) 1.
24. G. Khalaj, M.J. Khalaj, *Int. J. Pres. Vessel. Pip.,* 145 (2016) 1.
25. M.Wu, F. Xie, X. Chen，D. Wang, Z.J. Diao, W.J. Zhang, L. Ge, *J. Sichuan Univ.(Eng. Sci. Ed*.), 45 (2013) 185.
26. F. F. Eliyan, A. Alfantazi, *Corros. Sci*., 74 (2013) 297.
27. R. Cabrera-Sierra, I. Garia, E. Sosa, T. Oropeza, I. Gonzalez, *Electrochim. Acta*, 46 (2000) 487.
28. J. Luo, Y. Zhang, Q.D. Zhong, L. Zhang, Z.Y. Zhu, *Corros. Prot*., 33 (2012) 349.
29. C.W. Li, Z.Q. Cao, C.Y. Zheng, Y.S. Lu, Q.Y. Tian, *J. Shenyang Normal Univ(Nat. Sci. Ed.).,* 32 (2014) 156.
30. K. Ralston, N. Birbilis, C.H.J. Davies, *Scr. Mater*., 63 (2010) 1201.
31. S. Gollapudi, *Corros. Sci*., 62 (2012) 90.
32. Z.Y. Qi, J. Wen, R.Xu, X.P. Fang, G. Cui, Z.L. Li, *Corros. Prot*., 40 (2019) 190.
33. M. Zhang, L. Li, K.K. Cheng, Y. Wang, J.H. Li, *Ordnance Mater. Sci. Eng*., 41 (2018) 1.
34. Z.Q. Cao, W.H. Liu, Z.G. Zheng, Y. Niu, *Chin. J. Nonferrous Met*. 16 (2006) 170.
35. Z.Y. Liu, Z.S. Li, X.L. Zhan, W.Z. Huangfu, C.W. Du, X.G. Li, *Acta Metal. Sin.,* 52 (2016) 965.